

## DESIGN ANALYSIS OF THE NEW LANL 4-ROD RFQ

S.S. Kurennoy, E.O. Olivas, and L.J. Rybarczyk, LANL, Los Alamos, NM 87545, USA

### Abstract

An upgraded front end of the LANSCE linac will include a 4-rod RFQ replacing the aging Cockcroft-Walton injector, initially only for protons. We performed a detailed analysis of the proposed RFQ design using 3D modeling with the CST Studio Suite. The CAD-based RFQ model takes all design details into account. The electromagnetic analysis with MicroWave Studio (MWS) is followed by beam dynamics modeling with Particle Studio (PS) using the MWS-calculated fields. In addition, a thermal and stress analysis is performed with ANSYS, based on the power flux from MWS computations. Simulation results are used for design iterations aimed to satisfy special requirements imposed by an existing common transfer line for different beams injected into the 201.25-MHz drift-tube linac.

### INTRODUCTION

LANL is moving forward with replacing the aging Cockcroft-Walton (C-W) injectors with an RFQ-based front end [1] for the LANSCE proton linac. A 4-rod type RFQ design was developed in collaboration between IAP (Frankfurt) and LANL. The LANL RFQ, operating at 201.25 MHz at the duty factor up to 15%, with 35-keV injection and 750-keV final energy, should satisfy special requirements due to its incorporation into the existing medium-energy beam transfer that works with multiple beams, see in [2]. The RFQ will be manufactured by Kress GmbH. We used the RFQ CAD files from Kress imported into CST Studio [3] to create a model of the LANL  $H^+$  RFQ and evaluate its performance.

### RFQ MODEL

The imported CAD model was simplified by removing details nonessential for EM analysis such as external supports, etc. The RFQ cavity walls were also removed, leaving only the resonator vacuum volume in the CST model. The resulting model is shown in Fig. 1. Here the RFQ vacuum vessel, in light-blue, is 175-cm long (wall-to-wall), 34-cm wide, and 30-cm high (along the stem direction,  $z$ ). It also includes wide recesses on the thick end and front walls, of radius 8.5 cm and depth 1.5 cm, followed by 5-cm-long beam pipes of radius 2 cm. The RFQ vanes are supported by 24 stems that are spaced longitudinally with variable period, 75 mm in the center and 69.5 mm for three periods near each end. The tuners electrically short two adjacent stems and can be moved along them (in  $z$  direction) to adjust the mode frequency and voltage profile (flatness) along the structure length. The variable stem spacing simplifies tuning the voltage flatness along the structure. Our RFQ model uses the CAD model coordinates:  $x$  is along the RFQ axis, and the beam is moving in  $-x$  direction (right to left in Fig. 1).

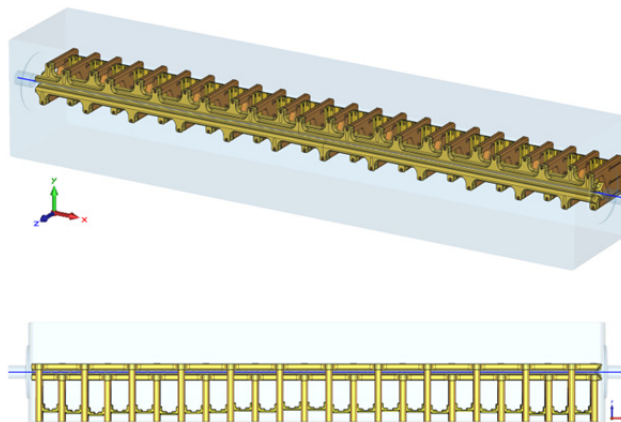


Figure 1: RFQ model (top) and its side view (bottom).

One can see in Fig. 1 (bottom) that the tuners are at different heights: they are adjusted to make the inter-vane voltage flat within  $\pm 1\%$ . However, even with all tuners at the same height, the voltage is flat within  $\pm 5\%$ , due to the variable stem spacing.

### ELECTROMAGNETIC ANALYSIS

We studied the RFQ model using the CST MicroWave Studio (MWS). The mode frequencies and RF fields are calculated by the AKS eigensolver that provides more accurate surface approximations. The RF fields have some interesting features resembling those found in the FNAL 4-rod RFQ, see in [4, 5].

The first is the presence of a small transverse horizontal (parallel to the ground plane) electrical-field component,  $E_y$ , on the RFQ geometrical axis, sometimes referred to as a “dipole” component. This is due to the transverse electric fields being stronger between two upper vanes than between two lower ones, which results in the center of the transverse quadrupole field displaced down, to the ground plane, from the geometrical axis by 0.45 mm. The shift is small but not negligible when compared to the 4-mm vane aperture. This effect is known in 4-rod RFQs designed for higher frequencies [6]. The electric-field components on axis: longitudinal  $E_x$ , horizontal  $E_y$ , and vertical (along the stems)  $E_z$  are plotted in Fig. 2 versus the longitudinal coordinate  $s = -x$ . The fields are scaled to the nominal inter-vane voltage  $V_0 = 50$  kV. In a similar plot along the axis shifted by -0.45 mm in  $z$ , the horizontal component  $E_y$  is close to zero, while the other two do not change much compared to Fig. 2.

Another important feature is the longitudinal electric field in the end gaps that separate the vane ends from the RFQ box walls (end-gap bumps). The red curve  $E_x$  in Fig. 2 shows the RFQ accelerating field – the oscillating part – produced by the vane modulation. The curve also has two peaks, near the entrance and exit.

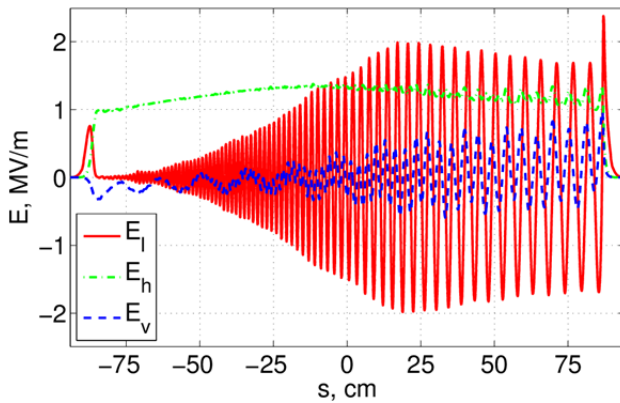


Figure 2: On-axis electric field in the RFQ model.

The RFQ cavity extends from  $s = -87.5$  cm to  $s = 87.5$  cm; the vanes start at  $s = -86.9$  cm and end at  $86.9$  cm. It would make 6-mm gaps; however, the gaps are effectively wider by 1.5 cm due to the recesses cut out in the end walls and the beam pipes. This is why the entrance-gap peak of the longitudinal field is small. The large near-exit peak is due to a special end-vane design: one pair ends at a modulation maximum, another at minimum.

The end-gap longitudinal field exists because the quadrupole symmetry is broken near the RFQ ends; it would vanish in a perfectly symmetric structure. Moreover, in the end-gap areas there are transverse field components in addition to the usual quadrupole ones. Under some circumstances the end-gap fields, which are neither predicted nor taken into account by standard RFQ design codes, can change the exiting beam parameters such as energy and emittances [4, 5].

One important requirement for the RFQ operation is the inter-vane voltage flatness along the structure. The relative voltages, calculated at the midpoints of all 23 full periods, are presented in Fig. 3 for two cases: all tuners are at the same height, only the frequency is tuned to 201.25 MHz (“initial”) and after some tuner adjustments in the MWS model (“tuned”). Even for the initial profile, the voltage was reasonably flat, within  $\pm 5\%$  of the average value; this is due to the variable stem spacing.

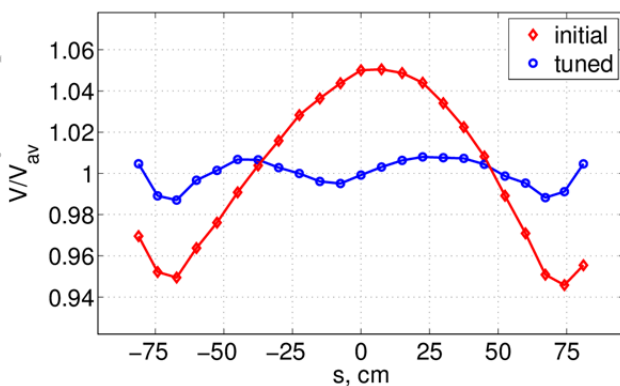


Figure 3: Voltage profile along the RFQ structure.

When all 23 tuners are moved together, by distance  $h$  up from the ground plane, the frequency sensitivity is  $df/dh = 0.75$  MHz/mm. The frequency tuning range is comfortably sufficient in this design. In the shown tuned case, the displacements of individual tuner plates range from -9.5 mm to 8 mm.

The calculated maximal field at nominal voltage  $E_{\max} = 23.5$  MV/m ( $1.6E_K$ ) is reached near the vane exit end. We use the fields calculated in the tuned case for our macro-particle simulations, and the related heat flux for thermal-stress analysis.

## BEAM DYNAMICS RESULTS

The RF fields calculated by MWS are imported into the Particle Studio (PS) PIC solver. For macro-particle simulations, we used “matched” distributions generated with LAACG codes [7]. Matched CW proton beams of 10K macro-particles, one RF period long, were generated for a few different currents at the model boundary from Twiss-parameters that were back-traced from the match point at the RFQ vane entrance. The resulting distributions are converted to CST PS format and injected for 10 RF periods at 35 keV, ( $\beta_{\text{in}} = 0.0086$ ), and accelerated to 750 keV, corresponding to  $\beta_{\text{out}} = 0.04$ . As an illustration, Fig. 4 shows macro-particles in the PS model with 12-mA current at  $t = 405$  ns after the injection of  $10 \times 10K$  particles started. The total number of macro-particles at this moment is about 97.4K, most of them are densely packed in bunches. The particle energy is indicated by color; the energy scale is overlapped on the right. The particles propagate from right to left. More than 10 bunches are formed, due to the longitudinal space-charge push at the train ends; a few leading bunches in Fig. 4 are already accelerated and approaching the exit. Trailing low-energy particles are not captured in bunches.

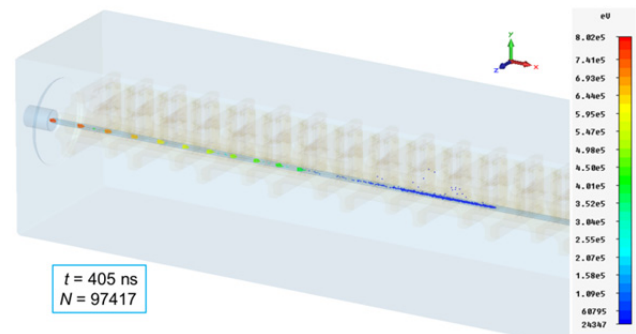


Figure 4: Particles in the RFQ model for 12 mA at 405 ns.

A convenient way to look at energy changes is with phase-space snapshots of the longitudinal phase space  $x-W$  (coordinate-energy). In Fig. 5, five such snapshots, from  $t = 405$  ns to 409 ns with 1-ns step, are overlapped. Each snapshot is shown in a different color; together they cover a time interval equal to one RF period. One can see that the bunch energy increases until the end of the modulations ( $x = -869$  mm), then remains constant in the

exit beam pipe ( $x < -890$  mm). Again, the beam propagates from positive to negative  $x$  in this model.

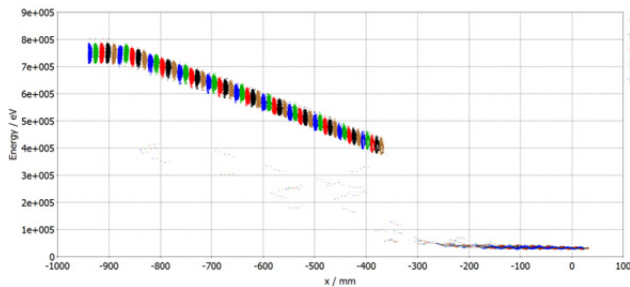


Figure 5: Longitudinal phase-space snapshots for 12 mA.

To exclude effects of space charge in the bunch-train head and tail, we analyzed only 4-6 central bunches from PS simulations with  $10 \times 10^6$  beams injected. Some results – the average energy  $W$  of exiting bunches, their transverse normalized r.m.s. emittance  $\epsilon_t$ , and current transmission – are summarized in Table 1. The initial distribution has a transverse normalized r.m.s. emittance  $0.2 \pi$  mm·mrad in both transverse planes.

Table 1: PS Results for Different Beam Currents

$I$ , mA	$W$ , keV	$\epsilon_t$ , $\pi$ mm·mrad	$\epsilon_b$ , keV·deg	transm.
0	756	0.40	20	0.99
12	756	0.55	13	0.97
35	753	0.62	15	0.89

The calculated growth of the transverse emittance, even in the matched low-current case, is large. On the other hand, the longitudinal emittances are smaller than expected. We consider the emittance results preliminary and will investigate this problem further.

### THERMAL ANALYSIS

The total dissipated power in the RFQ model for ideal copper surfaces is 77 kW at 100% duty and is distributed as follows: 55% on stems, 28% on vanes, 17% on tuners, and less than 0.5% on the RFQ-vessel inner surface. Since the RFQ will operate at noticeable duty factors, up to 15%, the structure requires adequate cooling. It will be provided by water running at 2.5 m/s through cooling channels. Each stem has a separate inverse-V-shaped cooling channel. There are also cooling channels inside vanes, connected through a few stems to pipes under the ground plane. The heat flux calculated in post-processing MWS fields was used for thermal-stress analysis with ANSYS [8].

In the thermal analysis, a realistic contact copper-copper conductivity between vanes, stems, and tuners was taken into account. The calculated temperature distribution in a structure slice near the RFQ exit is shown in Fig. 6 for the duty of 18% (15% plus additional heating due to realistic surface conductivity). The maximal

temperature of 335 K is at the near-end stem and the temperature range is less than 40° C even in this extreme case. Maximal deformations in the RFQ structure reach 80  $\mu$ m but the relative vane displacements stay below 40  $\mu$ m ( $< 0.002''$ ).

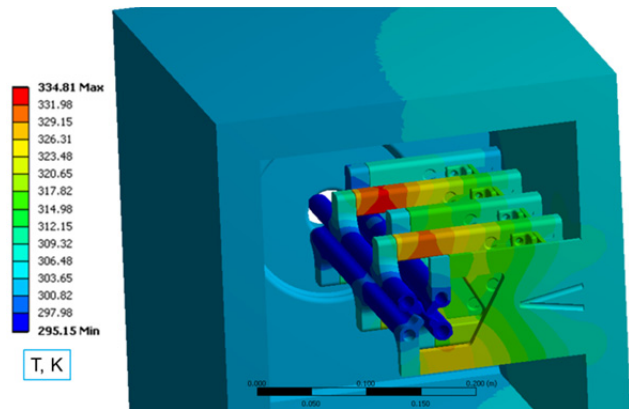


Figure 6: Temperature distribution at 18% duty.

### SUMMARY

A detailed study of the new LANSCE 4-rod RFQ was performed with the CST Studio codes. The RFQ model is based on imported CAD files. The RF fields calculated with Microwave Studio were used for beam dynamics modeling with Particle Studio and for thermal-stress analysis with ANSYS. Our modeling takes into account effects associated with 3-D field asymmetries such as end-gap fields, which are not predicted by standard RFQ design codes. We found that the RFQ output energy and transmission satisfy the design requirements and that the structure cooling is adequate. Reasons for the observed transverse emittance growth will be further investigated.

The authors would like to thank A. Schempp and J. Schmidt (IAP, Frankfurt), J. Haeuser (Kress GmbH), and Y. Batygin, R. Garnett, and J. O’Hara (LANL) for useful information and stimulating discussions.

### REFERENCES

- [1] R.W. Garnett et al, “Status of LANSCE RFQ front-end upgrade,” MOPMA14 NA-PAC’13.
- [2] L.J. Rybarcyk et al, “Design requirements and expected performance of the new LANSCE H<sup>+</sup> RFQ,” MOPMA17 NA-PAC’13.
- [3] CST Studio Suite, CST, 2013, www.cst.com
- [4] S.S. Kurennoy et al, IPAC13, Shanghai, China, THPWO094, p. 3978 (2013); www.JACoW.org
- [5] S.S. Kurennoy, reports LA-UR-12-26388 and LA-UR-13-21653, Los Alamos, 2012-2013.
- [6] B. Koubek et al, PAC11, New York, p. 1888 (2011).
- [7] Los Alamos Accelerator Code Group, laacg.lanl.gov
- [8] ANSYS, ANSYS Inc., www.ansys.com